The Atmospheric Structure During Episodes of Open Cellular Convection Observed in KonTur 1981

G. Kruspe and S. Bakan

Max-Planck-Institut für Meteorologie, Hamburg, Federal Republic of Germany

The KonTur (Konvektion und Turbulenz) 1981 experiment was primarily dedicated to the study of organized boundary layer convection. While two research aircraft were used for detailed boundary layer measurements, an aerological network of four stations in the North Sea yielded information on the mean atmospheric structure in organized convective situations. During the second experiment phase in October 1981, cold air advection caused intense convective activity. Four periods of well-organized open convection cells could be determined from NOAA satellite images. The present paper contains the results from the aerological data set, which allowed the derivation of mean profiles of the dynamic and thermodynamic quantities with acceptable accuracy, but also of the horizontal gradients of thermodynamic quantities. Finally, the evolution of the most pronounced cellular episode is presented in a case study. Cellular episodes appeared during rather cold and dry periods in which potential temperature, specific humidity, and equivalent potential temperature in the convection layer reached a relative minimum. However, none of the mean atmospheric profiles differ considerably from those found under convective conditions without cellular organization. During the cellular episodes, horizontal gradients show generally small values throughout the convection layer.

1. Introduction

Cold air advection over the sea is frequently accompanied by the organization of convective clouds into fairly regular structures (Figure 1). These are characterized by more or less ringlike cloud groups having a typical diameter of 30–50 km. The cloudy walls mark areas of average lifting of air due to a convectively driven secondary circulation, while the cloud-free interior is due to compensating subsidence.

Since the advent of meteorological observation satellites, this phenomenon has been repeatedly described and documented [e.g., *Krueger and Fritz*, 1961; *Agee et al.*, 1973; *Agee*, 1987]. The determination of quantitative data of organized open cellular convection events, however, turned out to be a difficult task. This is due to the mesoscale nature of the phenomenon, which occurs almost exclusively over the ocean. Satellite images yield information on the horizontal planform but cannot tell too much about the vertical structure. *Krueger and Fritz* [1961] evaluated several radiosoundings from routine stations in the subtropics when the satellite images showed open cellular convection. They found an adiabatically stratified layer of moist air about 1500 m deep, heated from the ocean, which was capped by a layer of greater stability. Throughout the convective layer there appeared to be little variation in wind speed and direction. Furthermore, they noted a typical diameter to depth ratio of about 30, as opposed to values of 2–3 for laboratory convection. This discrepancy is not yet really understood, although various tentative explanations have been put forward [*Priestley*, 1962; *Sasaki*, 1970; *Rosmond*, 1973; *Rothermel and Agee*, 1986; *Chlond*, 1988].

During the Air Mass Transformation Experiment (AMTEX) 1974/1975 a dedicated study of organized convection in cold air outbreaks was possible for the first time [*Lenschow and Agee*, 1976]. *Sheu and Agee* [1977] report that the observed cases of open convection cells were associated with large-scale divergence (1.7×10^{-5} s^{-1}) and sinking, sea-air temperature differences larger than 5 K, and surface wind speeds above 5 m/s. *Agee and Lomax* [1978] found the height of the inversion base to be markedly lower in open cell cases than in areas of closed convection cells. The compositing of different ascents into a "thermodynamic" model of an open cell indicated that relative humidity and inversion base height are larger, and potential temperature is lower, in the cloudy walls than they are in the cell center.

From satellite images and routine weather data from the Chinese Sea, *Miura* [1986] derived the convection height, aspect ratios, and layer stability in several cases of organized convection (rolls and cells) in cold air outbreaks. He found an increase of static stability, relative humidity, layer depth, and cell aspect ratio with the downwind distance from the coast. In accordance with theoretical studies the cell aspect ratio turned out to be proportional to a layer-averaged Rayleigh number, and to be larger the closer the environmental lapse rate is to the moist adiabatic lapse rate.

Similar statistical studies of the appearance of cellular patterns and their relations to various boundary layer characteristics in the northeast Atlantic have been reported by *Busack et al.* [1985] and *Bakan and Schwarz* [1988]. Their results were derived from the inspection of simultaneous NOAA satellite images of the northeast Atlantic area, and routine surface and aerological data from the Weathership M (65°N, 2°E) for the period 1980–1983. Average air-sea temperature differences of -4.7 ± 2.4 K and wind speeds of 11.1 ± 4.8 m/s were found during situations of open cellular convection with according sensible and latent heat fluxes of 89 ± 55 and 138 ± 65 W/m. The horizontal divergence in the surface layer was considerably smaller than values reported for AMTEX but showed large variability ($0.12 + 1.01 \times 10^{-5}$ s^{-1}). On the yearly average, about 10% of the northeast Atlantic area was covered by open cells. Due to the large average vertical heat flux this area provides 20% of the total annual surface heat flux into the atmosphere. South of 60°N the most abundant cell diameters were 50–60 km, while
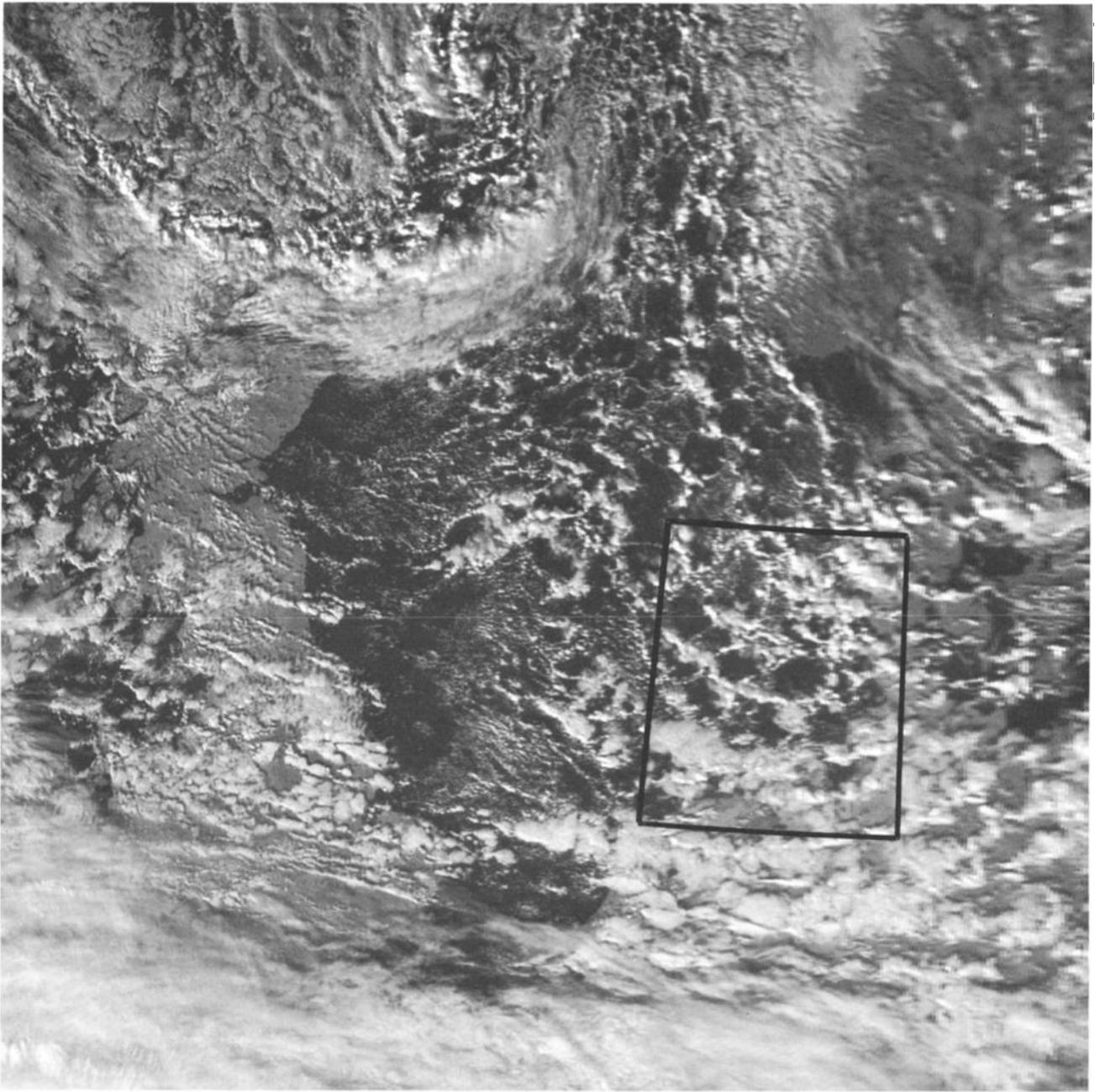
Fig. 1. Open cellular convection over the North Sea during the experiment KonTur 1981 (NOAA 7, October 14, 1424 UT). The black box represents the experiment area shown in Figure 2.

north of 70°N, cells of 20–30 km diameter prevailed. The aspect ratios derived were almost independent of the air-sea temperature difference, of the convection layer depth, and of the temperature lapse rate. The observed cellular pattern tended to become more regular at larger total heat fluxes.

The KonTur (Konvektion und Turbulenz) 1981 experiment was dedicated to the study of boundary layer processes, especially of organized convection [*Hoeber*, 1982; *Hinzpeter*, 1985; *Brümmer et al.*, 1985]. An aerological network with four ship stations and two research aircraft allowed a detailed study of the atmospheric structure during the experiment. Fortunately, during part of the experiment, cold air advection led to several phases of open convection cells. While the results of the aircraft studies have already

been reported [*Brümmer et al.*, 1986], the present paper contains information on the atmospheric structure during these cellular episodes as derived from the aerological data set.

2. THE KONTUR EXPERIMENT

The KonTur experiment took place during September/October 1981 over the North Sea, the main goal being the study of convection and turbulence in the marine boundary layer. Figure 2 shows the experimental area in the North Sea together with the four radiosonde stations on board two research and two light vessels. The two participating aircraft (British Hercules C-130 and German Falcon-20) operated
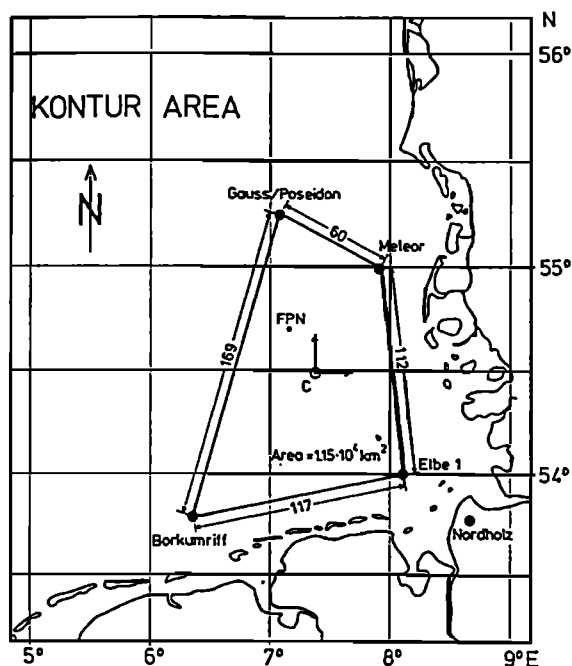
Fig. 2. The network of aerological stations (C is the center of the experiment area; FPN is Forschungsplattform Nordsee) and their mutual separations in kilometers.

from the airport at Nordholz. The experimental setting has been described in detail in a field phase report [*Hoeber*, 1982]. The primary purpose of the radiosonde program was to observe continuously throughout the experiment the mean thermodynamic and kinematic quantities [*Kruspe and Bakan*, 1988].

During the second phase of the experiment a period of cold air advection contained four episodes of well-expressed open cellular convection over the North Sea. This situation provided a unique opportunity to study the phenomenon rather thoroughly using two research aircraft and a network of surface and radiosonde stations. While the aircraft allowed us occasionally to study field properties of the meso-beta scale down to single cellular events, the surface and radiosonde network yielded the mean tropospheric conditions during convective situations.

3. AEROLOGICAL MEASUREMENTS

The following four ship stations formed the KonTur aerological network in the North Sea (Figure 2): Borkum Riff (53.8°N, 6.4°E), Elbe 1 (54.0°N, 8.1°E), Meteor (55.0°N, 7.9°E), and Poseidon (55.2°N, 6.1°E). While the latter two stations were located far enough from the coast to represent pure marine conditions, the former are light vessels residing at a distance of around 25 km from the coast line. Logistics constrained us to use these stations although coastal influence on the wind field had to be taken into account. The four stations followed a radiosonde launch schedule consisting of four soundings on normal days and 8–12 per day during intensive experiment phases. During periods of strong winds it turned out to be extremely difficult to keep up with the planned schedule, due to problems with the balloon handling. Nevertheless, the resultant aerological data set should

yield reliable horizontal averages as well as gradients of thermodynamic quantities down to periods around 6 hours.

At the ship stations (except for the R/V *Meteor*), Vaisala aerological setups of the First GARP Global Experiment (FGGE) type were deployed. These were to a certain extent "black boxes," providing no real-time data readout. At the R/V *Meteor*, the aerological equipment was a Vaisala Micro-Cora system, which proved to be very useful for control purposes and real-time data displays. Vaisala radiosondes of the type RS20 were used at all four sites.

Winds were obtained by navaid wind finding, which provides the wind by reference to the global radio navigation aid system. According to the manufacturer, the rms accuracy of the resulting wind velocities is ~2 m/s for heights above 500 m. Root-mean-square accuracies of the thermodynamic quantities are, after correction of the radiation influence on the thermistor and of the self-heating effect of the Humicap, about 1 hPa for pressure (aneroid cell), 0.3 K for temperature (thermistor), and 8% for relative humidity (Humicap hygrometer).

Primary processing of the aerological data was done by using the Vaisala editing software, which eliminates noise from the data and checks that vertical changes of the various parameter values are within acceptable limits. In addition, obviously bad data are removed by manual intervention. Geopotential heights were recalculated after offset corrections of the surface pressure data. These offsets were determined by applying the North Sea objective analysis scheme of *Luthardt* [1985] on the Global Telecommunication System (GTS) network data.

The profiles were interpolated to 50-m height intervals and were vertically smoothed with a Hanning taper [*Jenkins and Watts*, 1968]. By interpolation of neighboring soundings, time series with hourly steps were created for each particular height. These data were smoothed by a running cosine taper over 4 hours on either side of the designated times and sampled in steps of 3 hours.

From these profiles, horizontal gradients of pressure, temperature, humidity, and wind were calculated by least squares fit methods, assuming a first-order plane. Temporal tendencies were determined by calculating centered differences between the profiles of the preceding and the subsequent time step. According to the measurement accuracies of single stations with mutual distances around 100 km, the rms errors of the horizontal gradients should be less than 5 hPa per 1000 km for pressure, 3 K per 1000 km for temperature, 3 g/kg per 1000 km for specific humidity, and 20 m/s per 1000 km for wind speed gradients. Additional uncertainty may be introduced in a convective situation by unpredictable and unrecoverable flight paths of the radiosondes in the vicinity of clouds. Therefore different histories of simultaneously launched sondes may lead to apparent gradients. These disadvantages should be considerably relieved by the dense launch schedule during intense observation periods and by applying the above mentioned data processing procedures.

4. SYNOPTIC CONDITIONS

The dominant synoptic features during the second phase of the KonTur experiment are clearly reflected by the time-height cross section of the horizontal pressure gradient field (Figure 3). The pressure gradient vectors, closely tied to
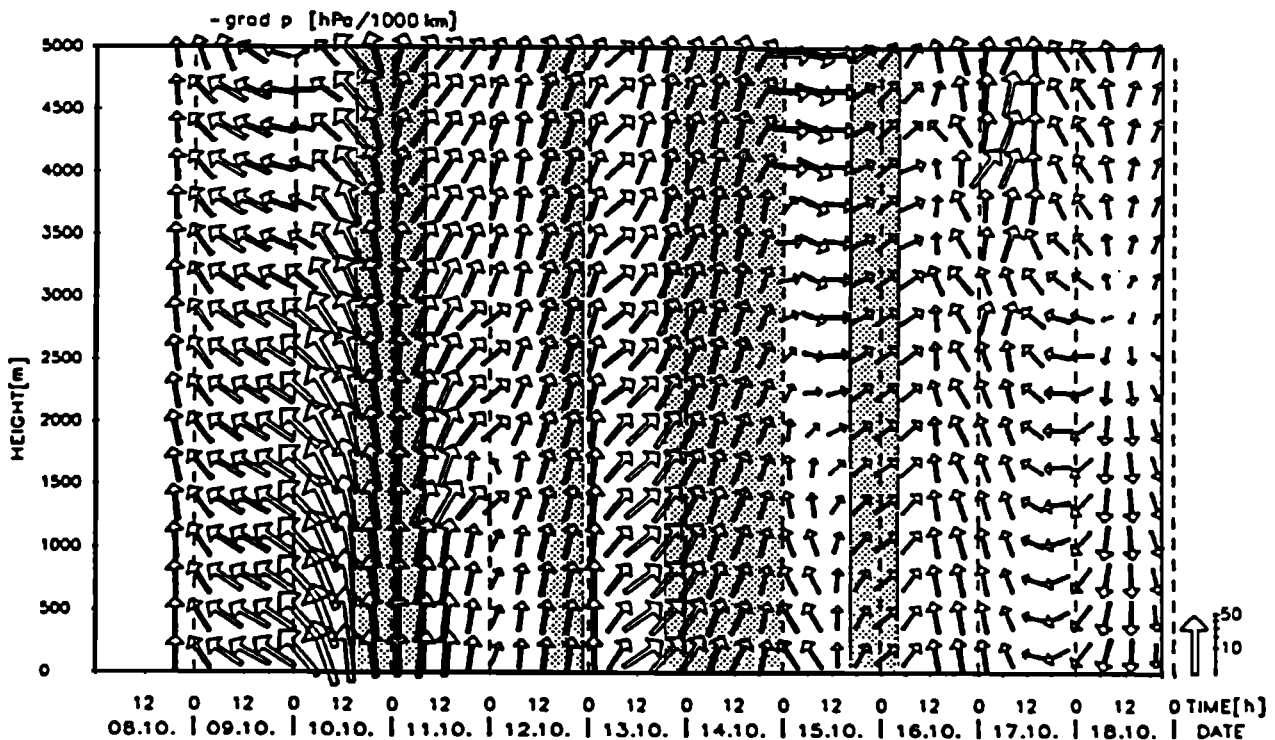
Fig. 3. Time-height cross section of pressure gradient field. The arrows refer to the orientation of the grad (p) vector, with the horizontal direction referring to the east and the vertical direction to north, pointing toward the low-pressure center. The length of the arrow on the right side is proportional to the magnitude of the horizontal gradient.

the evaluation of the wind field, are symbolized by arrows, which point in the direction of the steepest pressure decrease, with the horizontal direction referring to east and the vertical direction to north. Their lengths represent the value of the gradient in that particular direction.

Associated with the undulating, slowly southward moving, and mainly zonally aligned polar frontal zone near 60°N, intensive synoptic activity was initiated especially from October 9 to 14. During this time a gale type cyclonic depression moved eastward from near Ireland to the Norwegian sea, which is documented by the directional change of the arrows in Figure 3. This period was characterized by nonstationary conditions in the experiment area in which several frontal systems traveled eastward along the frontal zone over the North Sea. The resulting nearly periodic cold air outbreaks replaced the initially polar maritime air (October 9–12) with arctic maritime air (October 13) when the synoptic situation changed from cyclonic west to northwest. During this change a small depression center, coupled with trough development, suddenly originated in the North Sea. *Riehl* [1982] analyzed the thermal structure of this "warm low and trough" as a medium scale high-energy center, which passed the area between 0600 and 1200 UTC. From October 14 to 17 the synoptic situation changed to anticyclonic westerly flow.

Due to the intense synoptic activity, quasi-stationary periods prevailed for no longer than 20 hours in the KonTur area. Cold air surges were followed by interludes of relatively dry and stable air in which open cells of different regularity were observed as intermediate states.

5. RESULTS

5.1. Time Development at the Surface

The time development of the horizontally averaged surface data at 10 m height and that of derived bulk fluxes (Figure 4) represent the unstable convective conditions (z/L $\approx$ -0.3, $z = 10$ m; L is bulk Monin Obukhov stability length) during which four pronounced episodes of cellular events were identified.

The appearance of the convection cells and their state of organization were derived from NOAA satellite images, which were available every 6 hours. Individual satellite images have been assumed to represent the cloud pattern in the KonTur area for ± 3 hours around their receiving time. Four episodes of open cells were identified, of which the period from the evening of October 13 until the evening of October 14 showed the best organization with cell diameters of around 50 km (see Figure 1). In this latter case the cells could also be found over land, although they were less well expressed there.

Between October 10 and 16 the prevailing surface wind direction was from west to northwest. Initially high wind speeds around 15 m/s declined to values considerably below 10 m/s toward the end of the observation period. Advection of cool and dry air led to a situation in which the temperature of the ocean surface exceeded the air temperature by 3–5 K and rather low relative humidities around 70% were observed. This resulted in rather large turbulent fluxes of sensible ($H > 80$ W/m^2) and latent heat ($lE > 200$ W/m^2). The lifting condensation level, as derived from data at 10 m
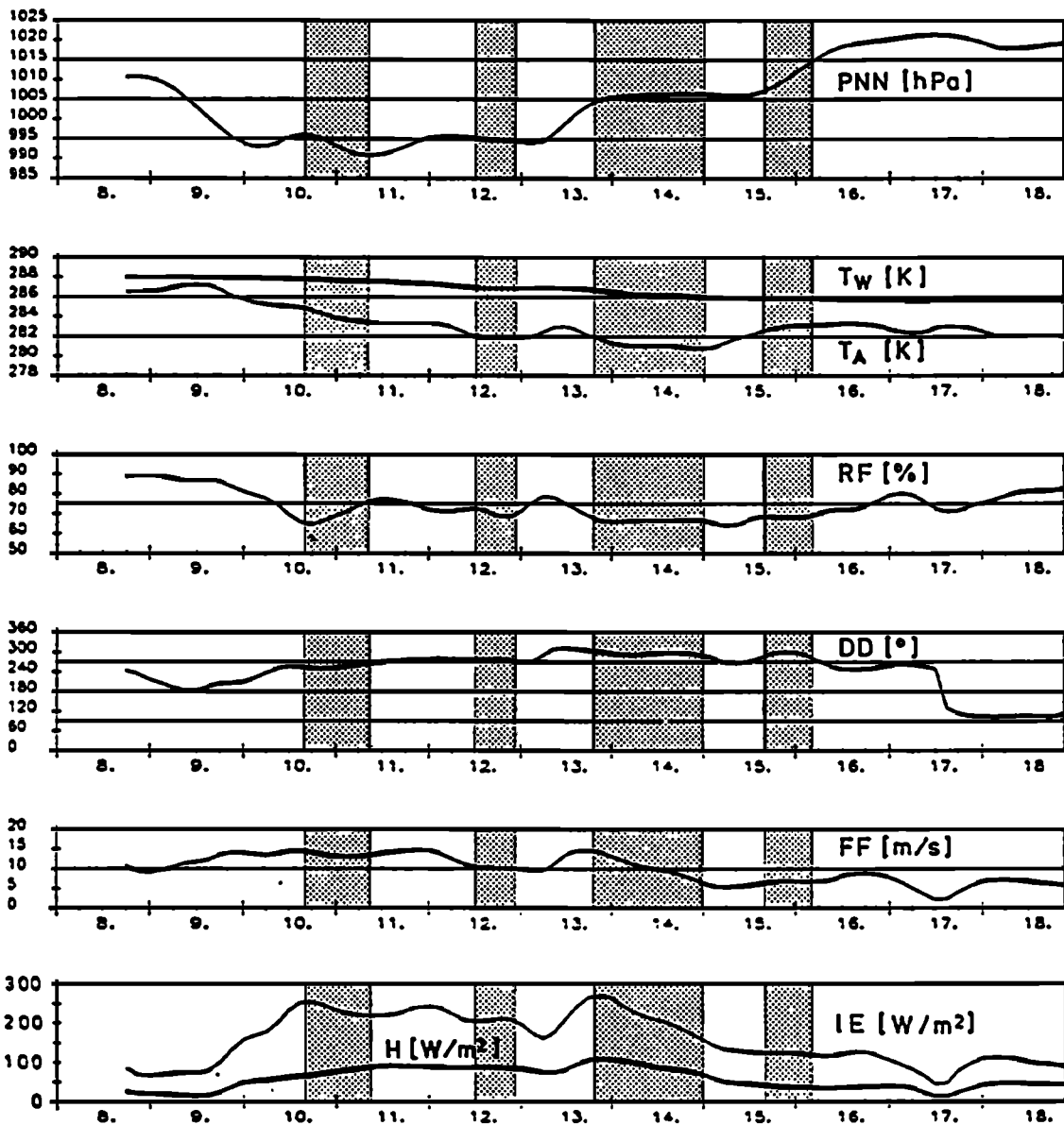
Fig. 4. Horizontally averaged surface data and synoptic events: P_{NN}, surface pressure; T_w, water bucket temperature; T_A, air temperature at 10 m height; RH, relative humidity; DD, wind direction; FF, wind speed; H, sensible heat flux; and lE, latent heat flux [after Liu et al., 1979]. Shaded areas indicate occurrence of organized convection.

height, was found to be between 500 and 800 m above sea level.

While all the data are characteristic of a convective boundary layer, the observed variability is not obviously connected with events of well-expressed cellular convection. A minimum sea-air temperature difference of 3 K is somewhat less than observed during AMTEX [Sheu and Agee, 1977] but fits into statistical findings of Busack et al. [1985] and Bakan and Schwarz [1988] for open cellular convection near Weathership M.

5.2. Time Development of Mean Fields

Time-height cross sections of various quantities have been produced from spatial averages of the soundings of at least two aerological stations smoothed with respect to time.

Many synoptic details may be recognized in Figures 5–10, which are of interest to the study of cellular events (shaded areas).

5.2.1. Thermodynamic quantities. The time development of thermodynamic quantities clearly reflects the cellular events.

Potential temperature: Potential temperature (Figure 5) may intuitively be believed to correlate best of all with the appearance of open cells. Indeed, the isentropes reach maximum values during the convective situations although not below 2.5 km in the last episode. Cold air surges are separated from warming phases by embedded quasi-stationary isentropic minima of different duration. These episodes were found to be quite in coincidence with well-expressed cellular organization. This was especially striking

Θ [K]
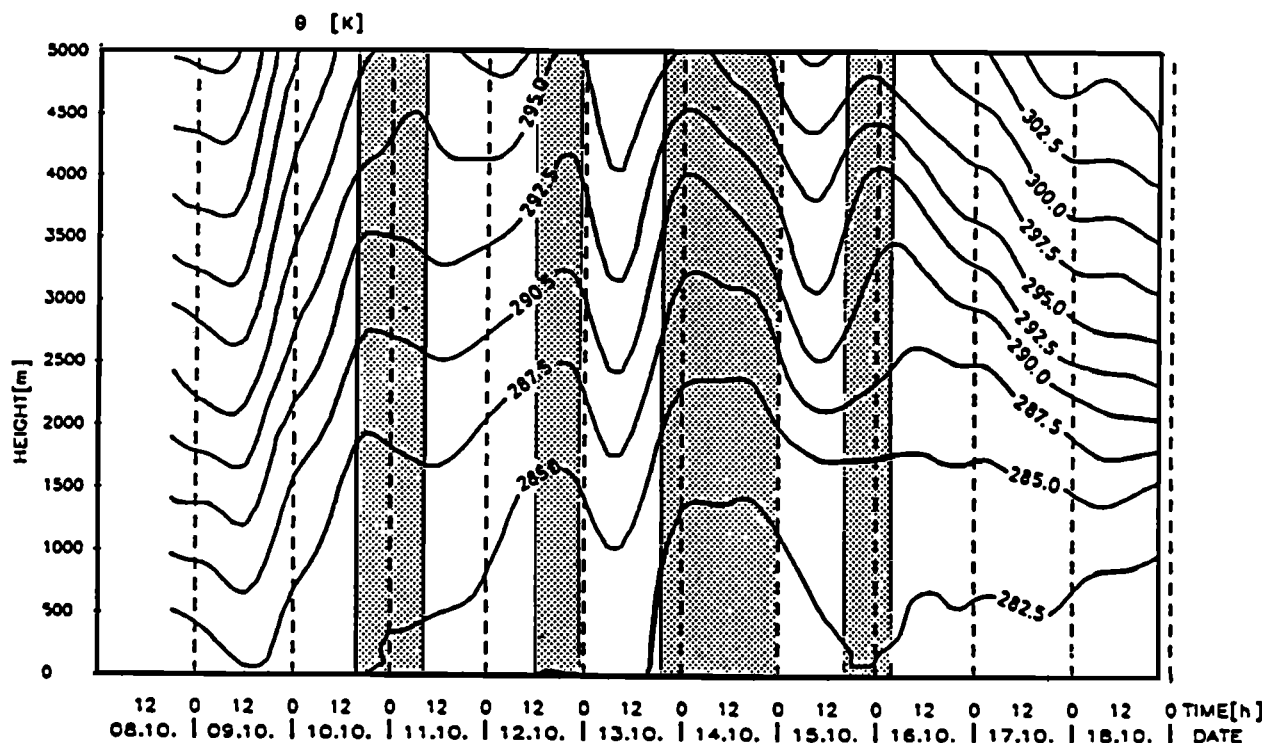
Fig. 5.   Time-height cross section of potential temperature (Θ in degrees Kelvin).

for the third phase of about 20 hours duration. Obviously, this indicates that well-expressed cellular convective structures may preferably exist in pools of rather stationary and horizontally homogeneous cold air.

Humidity: In reference to the four defined episodes of cold air invasion, cooling before the onset of cellular pat-terns is strongly correlated with drastically drying phases, as can be inferred from the steeply declining isolines of specific humidity in Figure 6. The local minima of these isolines coincide with the above mentioned cold air pools, in which cellular convection is best developed.

In contrast to specific humidity, the relative humidity field

q [g/kg]
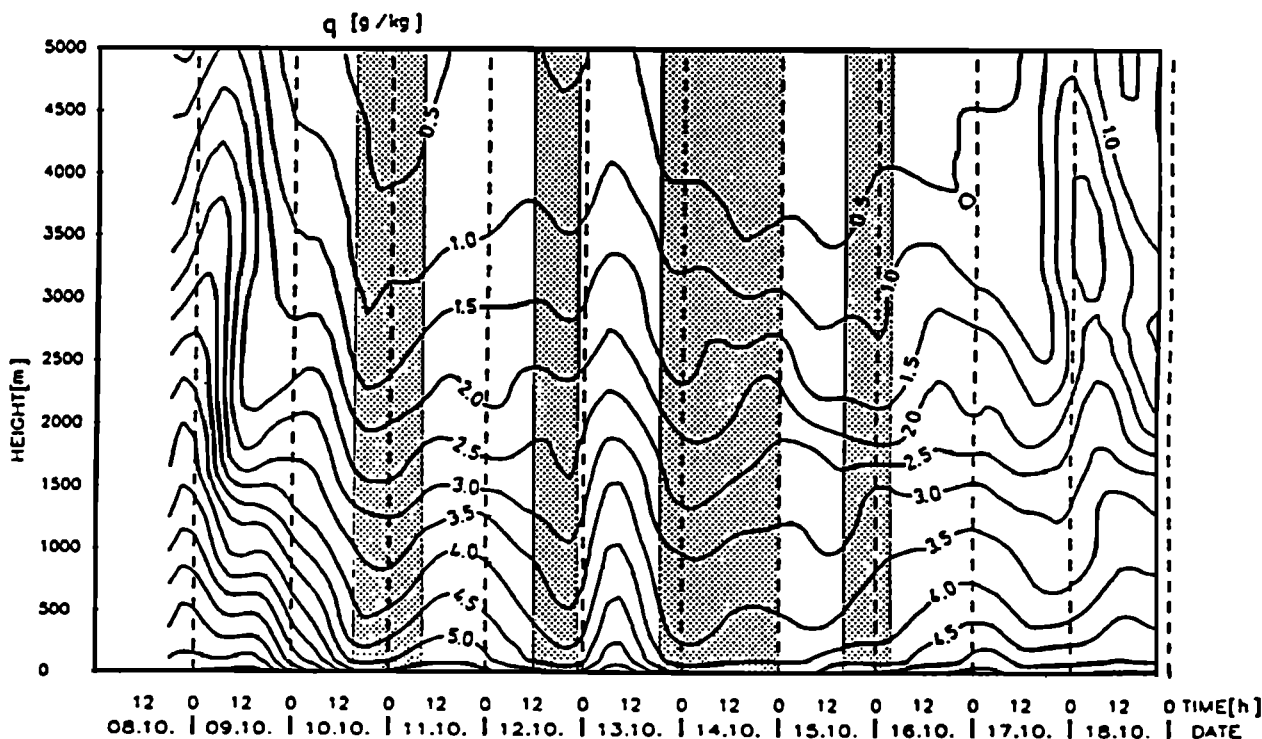
Fig. 6.   Time-height cross section of specific humidity (q in grams per kilogram).
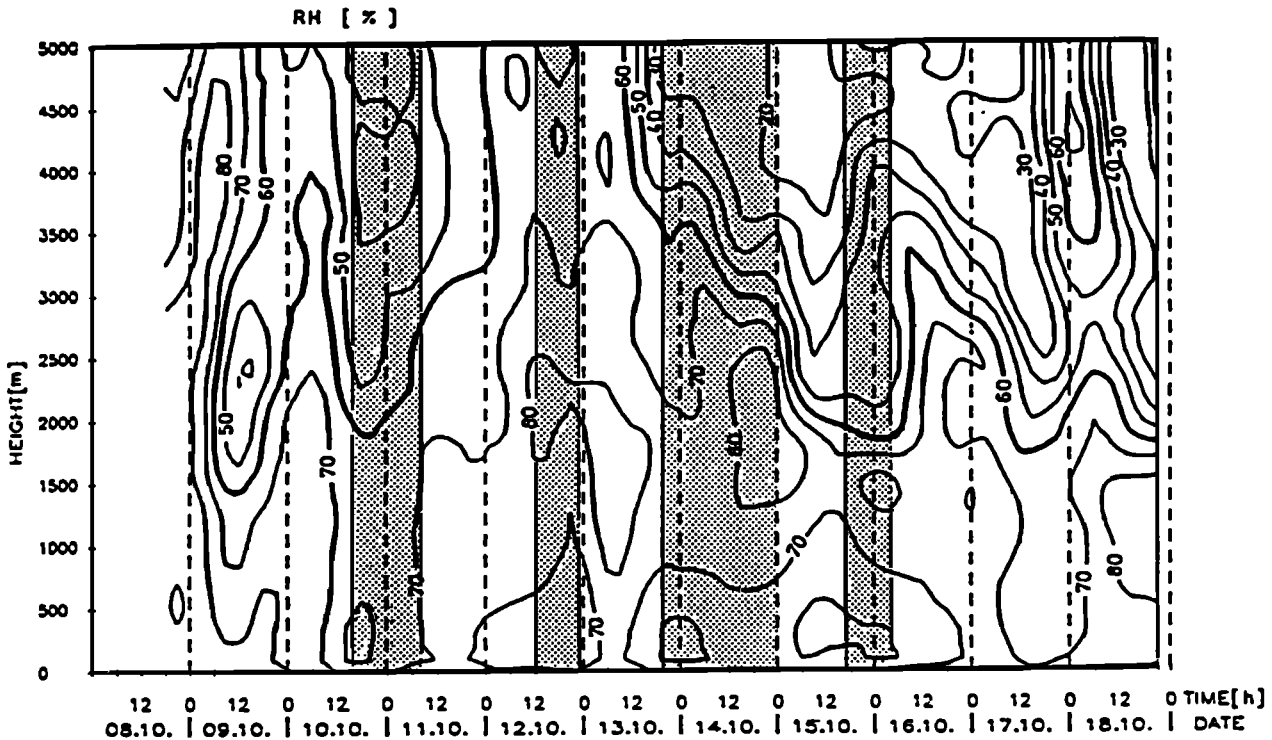
Fig. 7.   Time-height cross section of relative humidity (RH in percent).

(Figure 7) does not exhibit a very obvious relation to the individual cellular periods. But, better than either potential temperature or specific humidity, the relative humidity profile indicates the top of the convective layer by a usually pronounced reduction of the rather large boundary layer value to considerably reduced midtropospheric values. Therefore the evolution of the 60% isoline was chosen to represent at least qualitatively the development of the convective boundary layer height. Until October 12 the predominantly westerly cyclonic flow of maritime polar air is characterized by the growth of the moist layer depth from about 2 to 4 km. On October 13, deep convection occurred, so that relative humidities of more than 60% were found up to 5 km height. The anticyclonic influence, which set in on the evening of October 13, led to a successive decrease of the relative humidity in the middle and lower troposphere and, thus, of the convection height. Finally, the environment was modified sufficiently that the cells could no longer be supported.

Equivalent potential temperature: Equivalent potential temperature (Figure 8) is widely considered to be useful for air mass identification. While Θ_e increases almost monotonically with height at the beginning and end of the observation period, it represents a rather well mixed state throughout the lower 3–4 km in the period of cold air advection, indicating deep circulations in the boundary layer. In the preceding section, both potential temperature and specific humidity were found to exhibit relative minima during the occurrence of well-expressed cellular convection. Consequently, the mean field of equivalent potential temperature distinguishes those periods clearly by also showing a relative minimum of a few degrees. In the time-height cross sections these come out as remarkable (almost) closed isolines with the minima between 1500 and 2000 m height. These closed isolines

indicate an environment of quite stationary and horizontally homogeneous conditions. Also, the vertical variations are rather small within the convection layer while Θ_e increases above this layer. In the following the height of transition is considered as the depth of the convective layer.

The first and the third of the cellular episodes appeared after active cold frontal events, which are represented by a dense local pattern of nearly vertically aligned isolines. The other two cases follow passive cold air invasions after intermediate phases of slight warming. The end of each cellular episode is marked by an equivalent potential temperature increase due to advection of warm and moist air in subsident flow at the west side of transient ridges.

5.2.2.   Dynamic quantities.   While thermodynamic quantities exhibit characteristic common features during the cellular stages, neither wind speed (Figure 9) nor direction does so.

During well-expressed cellular phases, as well as during most of the second KonTur period, the vertical variation of wind speed in the convection layer was small, indicating the well-mixed state of the convective layer. Those active cold frontal events preceding cellular episodes 1 and 3 were coupled with high wind speeds which were rapidly decreasing during the cellular phases. In contrast, wind speed did not change considerably during cellular phases 2 and 4 and did not differ significantly from the wind speed before or after the events.

Systematic differences in wind speed and direction beneath about 0.6 km height from south (near the coast) to north (open sea) have been found during prevailing coast-parallel (westerly) flow, which indicates a coastal effect. The surface winds at the two southern platforms were typically 2 m/s less than for the two northern ones, and the wind directions at the former pointed about 5° further to the right.
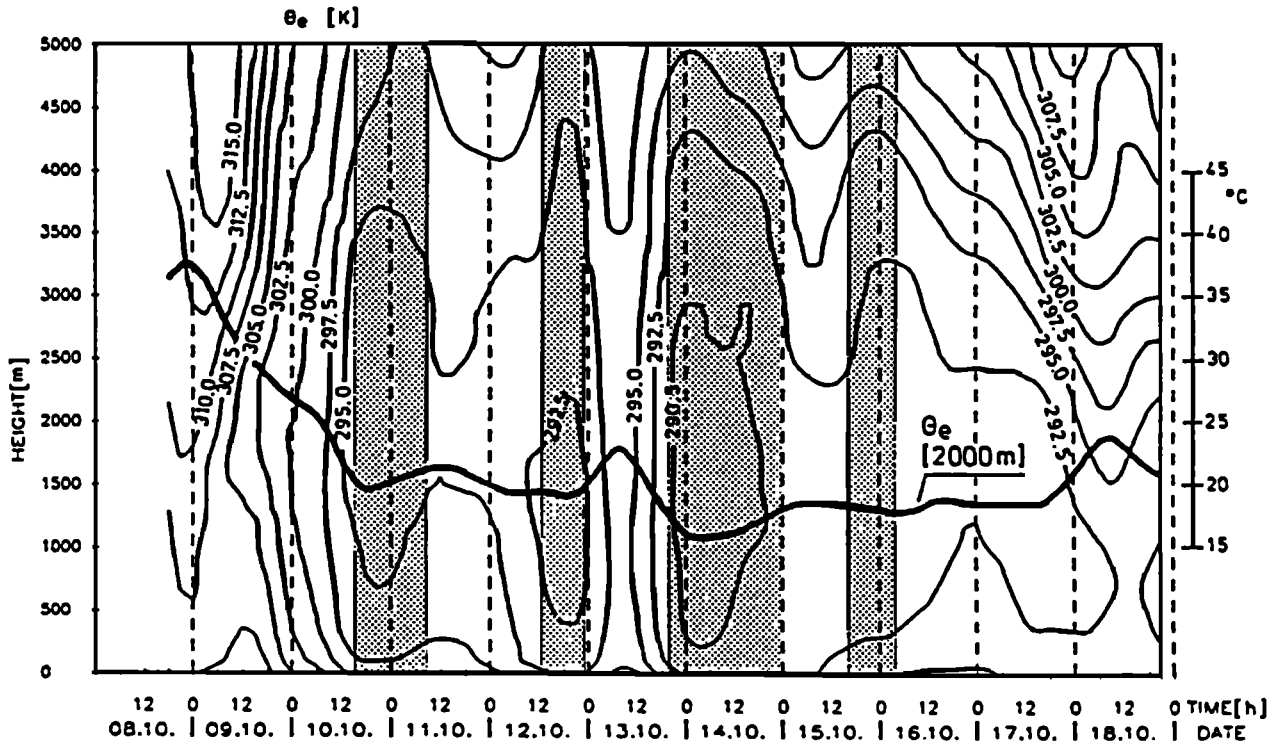
Fig. 8. Time-height cross section of equivalent potential temperature (Θ_e in degrees Kelvin).

5.3. Horizontal Gradients and Advection

Generally small gradients of the thermodynamic and dynamic quantities near the estimated accuracy limits are found except near the strong frontal events of October 9 and 13. Especially divergences do not exhibit any obvious correlation with the cellular periods. Due to the above mentioned accuracies in wind speed measurements (section 3) the divergence in cellular cases should be within $\pm 2 \times 10^{-5}$ s^{-1} throughout the convective layer. Below 500 m the flow tends to be convergent, probably due to coastal effects, which is consistent with the results of *Luthardt* [1985]. His objective analysis of routine surface data from the whole
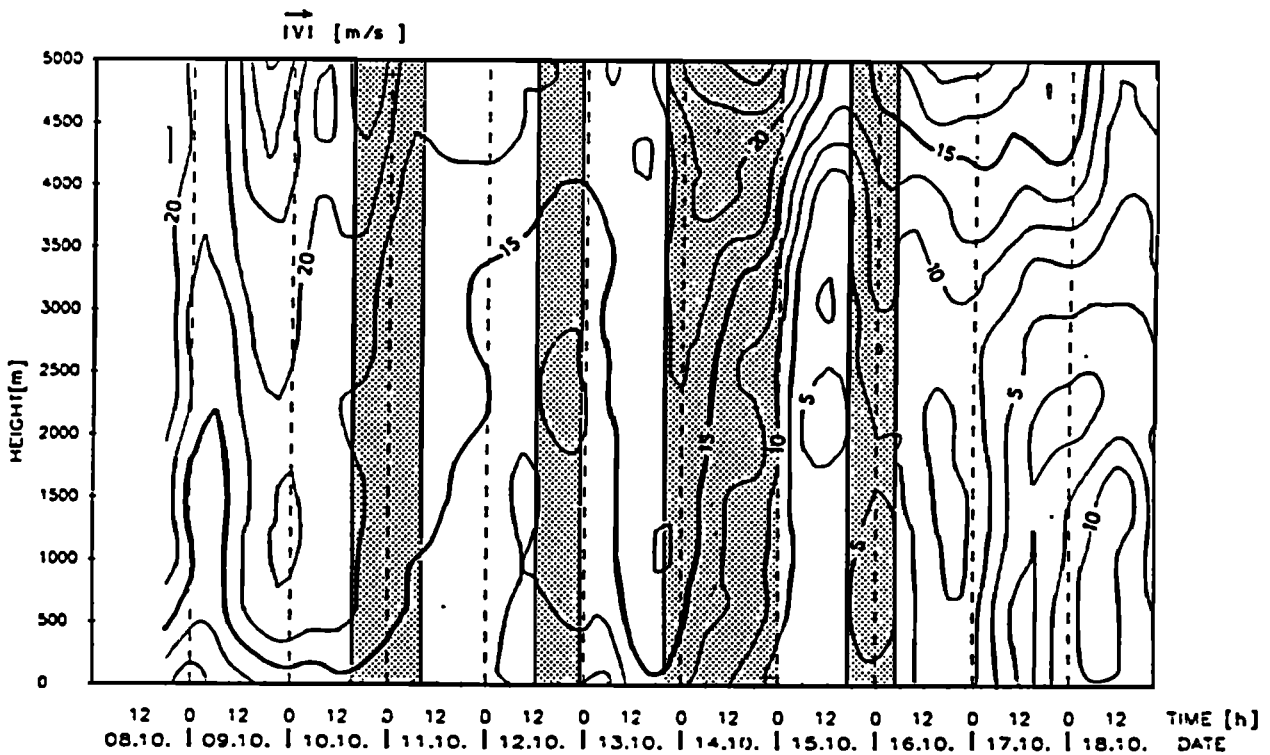
Fig. 9. Time-height cross section of wind speed ($|v|$ in meters per second).
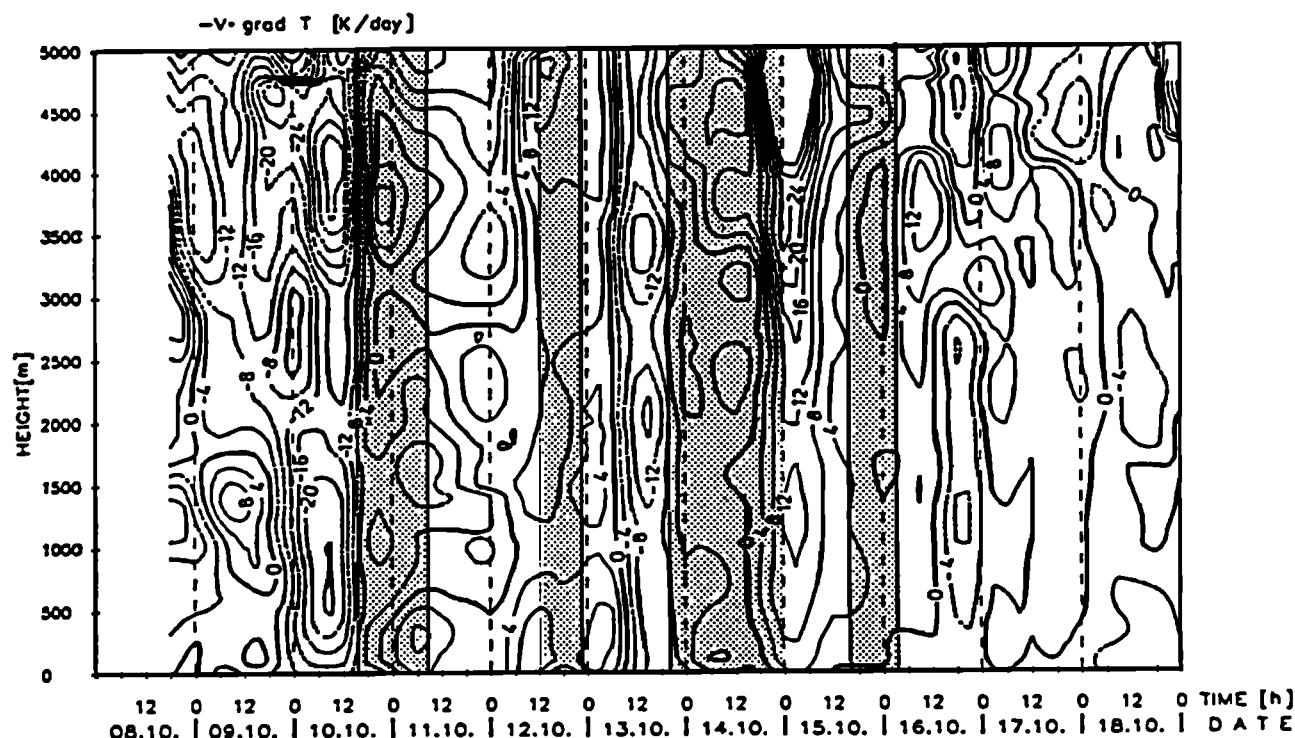
Fig. 10. Time-height cross section of horizontal temperature advection (in degrees Kelvin per day).

North Sea area shows coastal convergence in the southern part of the experiment area, too. It should be noticed that the divergence values found by other authors during open cellular convection (1.7 × 10⁻⁵ s⁻¹ by *Sheu and Agee* [1977] and $0.1 \pm 1.0 \times 10^{-5}$ s⁻¹ by *Busack et al.* [1985]) lie within the accuracy limits of our measurements.

Also, the horizontal moisture gradients and resulting moisture advection did not significantly exceed the measurement accuracy limits during most of this time. Advection resulted in drying rates >10 g kg⁻¹ d⁻¹ only during the initial period of strong cooling.

More significant details are revealed in the time-height cross section of the horizontal temperature advection (Figure 10), which should be accurate to within ±4 K/d. Small values are observed in the convective layer during the cellular periods. The first episode and the third episode are preceded by considerable advective cooling of the whole convection layer, and after the third episode, strong advective warming is observed. The other cooling and warming periods defined in Figure 6 represent rather small and slow temperature changes which are caused either by nonadvective processes or by temperature advection smaller than the mentioned accuracy limits.

5.4. Vertical Profiles During a Well-Expressed Cellular Phase

In this section the typical evolution of a cellular episode is documented by data from the best developed period on October 14. The observed mean vertical structures of several thermodynamic and dynamic quantities during the preceding (phase A: October 13, 0900–1800 UT), cellular (phase B: October 14, 0900–1800 UT), and succeeding (phase C: October 14, 2100 UT, to October 15, 0600 UT) development

stages are presented in Figure 11. These phases are separated by a few hours, as they were selected to be of equal length and to clearly represent the different development stages. While the thermodynamic quantities clearly reflect the cellular phase as opposed to the preceding and succeeding phase, the dynamic quantities are more governed by the synoptic development.

The vertical profiles of potential temperature are rather similar in all three phases below the cloud base. In the cloud layer the stability was found to be reduced during the organized convective phase B as compared to the other phases. Above 4000 m a progressive stabilization was observed.

The boundary layer was found during all three phases to be conditionally unstably stratified up to 1.5 km height. Also, the lifting condensation level does not show any striking change with time.

The profiles of Θ_e are quite similar during phases A and B up to 4 km height, above which, during the cellular phase, a more stable state prevails. This clearly corresponds to the humidity profiles, which show in phase A a secondary maximum that marks the levels of deeper convective clouds fairly well. In the cellular phase (B) the mean cloud top is around 3 km height. Phase C represents the progress of further stabilization and penetration of dry air into lower levels.

As is typical of open cellular conditions, the wind profile below 3 km height is rather constant without any striking vertical gradient during all phases. The absence of wind direction changes with height shows that there is no variation of thermal advection with height. But a noticeable increase in the layer mean wind speed from phase A through phase C is observable, which is due to the large-scale

PRECEDING   PHASE A : OCT. 13, 0900-1800 UT   ——
CELLULAR   PHASE B : OCT. 14, 0900-1800 UT   ——
SUCCEEDING PHASE C : OCT. 14, 2100-OCT. 15, 0600 UT ---
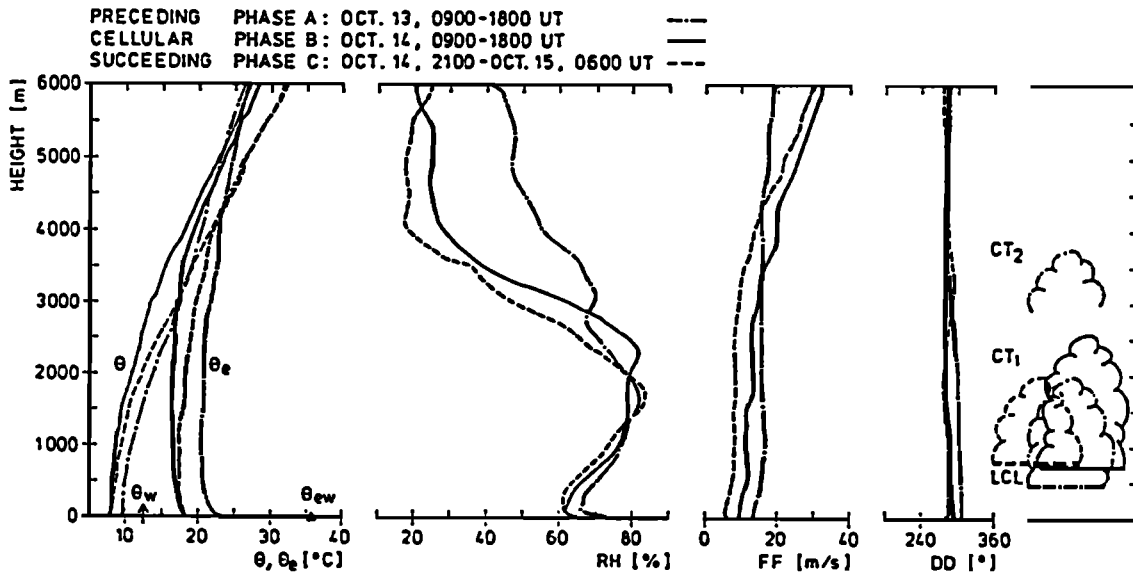
Fig. 11.   Mean vertical structure of several quantities before (phase A), during (phase B), and after (phase C) the best expressed cellular episode (T_w is water bucket temperature; Θ_{ew} is sea surface equivalent potential temperature).

development and obviously uncorrelated with cellular activity. Above the convection layer, increasing wind speed occurs together with increasing stability during phases B and C.

In Table 1, surface parameter values as well as tendencies and temperature advection are listed for several heights for all three phases, A–C. Phases A and B are characterized by large turbulent surface heat fluxes, which decreased during phase C due to the reduced surface wind speed.

Temperature tendencies were quite large during phases A (vertically increasing cooling) and C (vertically increasing warming) but insignificant up to 3 km height during the appearance of organized convection cells. With respect to pressure, there is a pronounced increase only during phase A

TABLE 1.   Selected Data Preceding, During, and Succeeding a Phase of Well-Expressed Cellular Activity on October 14, 1981

	Preceding Phase A			Cellular Phase B			Succeeding Phase C		
Surface									
ΔT, K	−4.5			−5.2			−5.0		
Δq, g/kg	−4.4			−4.8			−4.8		
FF, m/s	14.3			10.2			6.5		
H, W/m^2	113			93			55		
B	0.43			0.53			0.52		

	Preceding Phase A			Cellular Phase B			Succeeding Phase C		
	T, K	$|v|$, m/s	p, hPa	T, K	$|v|$, m/s	p, hPa	T, K	$|v|$, m/s	p, hPa
Tendencies per 3 hours									
10 m	−0.9	1.1	1.8	0.0	−0.8	0.0	0.5	−0.9	0.0
1000 m	−1.2	0.7	2.4	0.0	−1.4	0.0	0.5	−1.9	0.0
3000 m	−1.4	0.5	0.9	0.0	−1.1	0.2	0.7	−2.8	0.6
4500 m	−1.6	−0.6	0.6	0.5	0.4	0.5	1.2	−1.3	0.6

	Preceding Phase A	Cellular Phase B	Succeeding Phase C
Advection ($-v$ grad T), K/d			
10 m	−8	−3	3
1000 m	−6	0	8
3000 m	−12	0	15
4500 m	−10	5	20
div v, 10^5 s^{-1}			
10 m	−1.5	−0.5	0.0
1000 m	−2.0	0.0	−0.5
3000 m	−1.5	−0.5	−1.5
4500 m	−0.5	−2.0	−2.0

Here $|v|$ is wind speed, T is temperature, q is specific humidity, p is pressure, H is sensible heat, B is Bowen ratio (ratio of sensible and latent heat), and Δ indicates air-sea difference.

(inflow of denser cold air). Wind tendencies are generally positive in phase A and negative during phases B and C.

Thermal advection values indicate strong cooling in phase A and even stronger warming during phase C, but hardly any heating during the cellular phase B. The result underlines the important role of large-scale advection in the middle troposphere on the convective evolution.

The vertical structure of the boundary layer discussed in this section agrees qualitatively with the studies of, for example, *Krueger and Fritz* [1961] or *Agee and Lomax* [1978]: superadiabatic surface layer, dry adiabatic subcloud layer, moist adiabatic cloud layer, nearly vertically constant wind speed and direction throughout the convective layer, and stable stratification with changing wind above this layer. But it is evident that the vertical structure before and after the cellular episode also agrees qualitatively with the type of profile quoted in the literature for cellular events. This suggests that the observed vertical structure does not so much pertain to a situation of open cellular convection but rather characterizes cloudy convective boundary layers in general.

6. CONCLUSIONS

During the second phase of KonTur 1981, cold air advection led to intense convective activity in the experimental area with embedded events of well-organized cellular convection. The picture that emerges from the observed time series is as follows: Embedded in a cold air flow were various "pools" of even colder air showing up in the satellite images as areas with well-developed open cellular structure. These cold pools represent values of equivalent potential temperature smaller than prevail in the surrounding parts of the flow. They are characterized by small vertical gradients of wind speed and direction and of equivalent potential temperature. The conditionally unstable stratification of the boundary layer is consistent with the occurrence of cold dry air over warm water. Also, horizontal gradients of thermodynamic quantities were small, indicating strong vertical and horizontal mixing due to convective activity. Dynamic quantities, in contrast, did not exhibit significant variations throughout the passage of a cellular episode.

Although these cold pools are clearly discerned in the (free air) temperature record, the differences from the surrounding development phases are rather small. This is surprising, as the regular appearance of the phenomenon reveals it as a distinct mode of atmospheric secondary circulation. One would assume that such a remarkable atmospheric feature should require rather special circumstances in the larger-scale field for its appearance and/or should itself change the atmospheric field considerably during the development. A possible reason for this not being the case may be that the appearance of cellular organization depends on parameters not included in the present analysis or not determined with the necessary accuracy. Another possibility could be that, once initiated, organized cellular convection can persist even if the large-scale conditions become less favorable. Convective activity itself could remove an initially more unstable situation by intense vertical and horizontal mixing. *Huang* [1988] found such a "hysteresis" behavior in a mesoscale model of cellular convection.

The results of the present study suggest a few remarks on modeling. Most theoretical studies of organized convection

have been carried out with models of shallow layers in which simple, preferably linear profiles of the governing parameters could be assumed. But with an observed convection height of a few thousand meters, open cellular convection should represent a state of transition to deep convection. Therefore assumptions of, for example, a constant gradient of moist adiabatic temperature throughout the convection layer [e.g., *Asai and Nakasuji*, 1977; *van Delden*, 1985] are not valid, and related conclusions should be interpreted with care.

Many of these models assume a rigid lid model top, often representing the top of the convective layer. Our results show that such an assumption is weak, as the transition to the overlying stable layer is rather smooth. The height of the transition zone (which may be the relevant scaling height for the convection) may also vary throughout the convection cell, being higher in the walls and lower in the cell center, as was indicated by a compositing of routine AMTEX radiosoundings by *Agee and Lomax* [1978].

Although these more conceptual models give insight into physical mechanisms, quantitative comparisons with observations can only be expected from rather complete mesoscale models of the whole troposphere. An example of such a modeling attempt has been given by *Beniston* [1984, 1985] with a hydrostatic grid point model. When started with a stratification according to KonTur measurements and some initial disturbance the model produced regular structures of a few tens of kilometers diameter. Latent heat release was necessary for the onset of these structures. But with time the mean temperature and humidity profiles deviated considerably from the initial (observed) KonTur profiles, mainly due to the chosen cloud parameterization. Modern nonhydrostatic mesoscale models would certainly do a much better job, although even there the cloud parameterization for horizontal grid distances of a few kilometers poses a major problem.

Therefore model results should be able to explain not only the appearance of cellular convection but also the fact that it is not observed under rather similar atmospheric circumstances. The assessment of model performance becomes rather difficult, bearing in mind the small differences of environmental parameters that separate cases of well-organized and cases of not noticeably organized convection in our study. From our own experience with a further developed version of Beniston's hydrostatic model we know that a dedicated numerical model is able to produce cellular structures over a rather wide range of surface conditions and vertical profiles. Therefore an important test for the quality of such models is their ability to reproduce also such cases of similar atmospheric conditions but no noticeable convective organization.

REFERENCES

Agee, E. M., Mesoscale cellular convection over the oceans, *Dyn. Atmos. Oceans, 10*, 317–341, 1987.
Agee, E. M., and F. E. Lomax, Structure of the mixed layer and inversion layer associated with patterns of MCC during AMTEX 75, *J. Atmos. Sci., 35*, 2281–2301, 1978.
Agee, E. M., T. S. Chen, and K. E. Dowell, A review of mesoscale

cellular convection, *Bull. Am. Meteorol. Soc.*, *54*, 1004–1012, 1973.

Asai, T., and I. Nakasuji, A further study of the preferred mode of cumulus convection in a conditionally unstable atmosphere, *J. Meteorol. Soc. Jpn.*, *60*, 425–431, 1977.

Bakan, S., and E. Schwarz, Observations of cellular convection over the eastern Atlantic, *Rep. 16*, Max-Planck-Inst. für Meteorol., Hamburg, Federal Republic of Germany, 1988.

Beniston, M., A numerical study of mesoscale atmospheric cellular convection, *Dyn. Atmos. Oceans*, *8*, 223–242, 1984.

Beniston, M., Organization of convection in a numerical mesoscale model as a function of initial and lower boundary conditions, *Contrib. Atmos. Phys.*, *58*, 31–52, 1985.

Brümmer, B., S. Bakan, and H. Hinzpeter, KonTur: Observations of cloud streets and open cellular structures, *Dyn. Atmos. Oceans*, *9*, 281–296, 1985.

Brümmer, B., T. Fischer, and S. Zank, Aircraft observations of open cellular structures during KonTur, *Contrib. Atmos. Phys.*, *59*, 162–184, 1986.

Busack, B., S. Bakan, and H. Luthardt, Surface conditions during mesoscale cellular convection, *Contrib. Atmos. Phys.*, *58*, 4–10, 1985.

Chlond, A., Numerical and analytical studies of diabatic heating effects upon flatness of boundary layer rolls, *Contrib. Atmos. Phys.*, *61*, 312–329, 1988.

Hinzpeter, H., KonTur-results, *Contrib. Atmos. Phys.*, *58*, 1–3, 1985.

Hoeber, H. (Ed.), *KonTur—Field Phase Report, Geophys. Einzelschr., Ser. B*, vol. 1, Wittenborn, Hamburg, 1982.

Huang, X.-Y., On the hysteretic behaviour of moist convection, *Tellus, Ser. A*, *40*, 237–247, 1988.

Jenkins, G. M., and D. G. Watts, *Spectral Analysis and Its Applications*, Holden-Day, San Francisco, Calif., 1968.

Krueger, A. F., and S. Fritz, Cellular cloud patterns revealed by TIROS 1, *Tellus*, *13*, 1–7, 1961.

Kruspe, G., and S. Bakan, The atmospheric structure in cold air outbreaks during KonTur 81, *Rep. 13*, Max-Planck-Inst. für Meteorol., Hamburg, Federal Republic of Germany, 1988.

Lenschow, D. H., and E. M. Agee, Preliminary results from the air mass transformation experiment (AMTEX), *Bull. Am. Meteorol. Soc.*, *57*, 1346–1355, 1976.

Liu, W. T., K. B. Katsaros, and J. A. Businger, Bulk parameterization of air-sea exchanges of heat and water vapor including the molecular constraints at the interface, *J. Atmos. Sci.*, *36*, 1722–1735, 1979.

Luthardt, H., Estimation of mesoscale surface fields of meteorological parameters in the North Sea area from routine observations, *Contrib. Atmos. Phys.*, *58*, 255–272, 1985.

Miura, Y., Aspect ratios of longitudinal rolls and convection cells observed during cold air outbreaks, *J. Atmos. Sci.*, *43*, 26–39, 1986.

Priestley, C. H. B., Width-height ratio of large convective cells, *Tellus*, *14*, 123–124, 1962.

Riehl, H., Some features of northwest flow over the North Sea during the Kontur experiment, in *KonTur Preliminary Scientific Results, Geophys. Einzelschr., Ser. A*, vol. 57, pp. 25–44, Wittenborn, Hamburg, 1982.

Rosmond, T. E., Mesoscale cellular convection, *J. Atmos. Sci.*, *30*, 1392–1409, 1973.

Rothermel, J., and E. M. Agee, A numerical study of atmospheric convective scaling, *J. Atmos. Sci.*, *43*, 1185–1197, 1986.

Sasaki, Y., Influence of thermal boundary layer on atmospheric convection, *J. Meteorol. Soc. Jpn.*, *48*, 492–502, 1970.

Sheu, P. J., and E. M. Agee, Kinematic analysis and air-sea heat flux associated with mesoscale cellular convection during AMTEX 1975, *J. Atmos. Sci.*, *34*, 793–801, 1977.

van Delden, A., On the preferred mode of cumulus convection, *Contrib. Atmos. Phys.*, *58*, 202–219, 1985.

S. Bakan and G. Kruspe, Max-Planck-Institut für Meteorologie, Bundesstrasse 55, D-2000 Hamburg 13, Federal Republic of Germany.